

pubs.acs.org/JPCC Article

Four-Terminal Electrochemistry: A Back-Gate Controls the Electrochemical Potential of a 2D Working Electrode

Yuxin Wang and C. Daniel Frisbie*



Cite This: J. Phys. Chem. C 2024, 128, 1819-1826



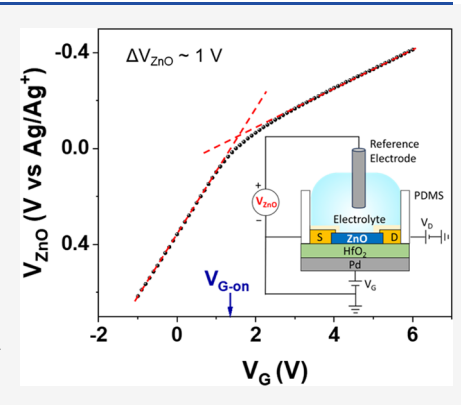
ACCESS I

III Metrics & More

Article Recommendations

SI Supporting Information

ABSTRACT: We demonstrate that ultrathin semiconductor working electrodes integrated into metal—insulator—semiconductor (MIS) stacks are an enabling platform for understanding non-Faradaic semiconductor electrochemistry. Here, 5 nm thick ZnO electrodes were deposited on 30 nm HfO₂ dielectric on a Pd "gate" electrode. Application of a bias $V_{\rm G}$ between the Pd gate and the ZnO electrode causes electrons to accumulate in the ZnO layer as measured by recording the in-plane sheet conductance. By contacting the top surface of the ZnO layer with the electrolyte in a conventional three-electrode electrochemical cell, we show that the gate voltage $V_{\rm G}$ modulates the electrochemical potential $V_{\rm ZnO}$ of the ZnO film with respect to a reference electrode. Electrochemical potential changes $\Delta V_{\rm ZnO}$ up to $-1~\rm V~vs~Ag/Ag^+$ are achieved for $V_{\rm G}$ = $+7~\rm V$. Furthermore, by measuring $V_{\rm ZnO}$ vs $V_{\rm G}$, we extract the quantum capacitance $C_{\rm Q}$ of the ZnO film as a function of the Fermi-level position, which provides a direct measure of the ZnO electronic density of states (DOS). Finally, we demonstrate that



the gated ZnO working electrodes can disentangle the two principal components of electrochemical potential, namely, the Fermi-level shift $\Delta\delta$ and the double-layer charging energy $e\Delta\phi_{\rm EDL}$. This disentanglement hinges on a fundamental difference between backgating and normal electrochemical control, namely, that electrochemical control requires double-layer charging, while back-gate control does not. Collectively, the results show that the backside gate electrode is an effective fourth terminal that enables measurements that are difficult to achieve in conventional three-terminal electrochemical setups.

INTRODUCTION

In recent work, we have demonstrated that the electric field effect can enhance the kinetics of electrochemical reactions at two-dimensional (2D) semiconductor working electrodes. 1-3 The essential concept is to integrate an ultrathin semiconductor electrode into a metal-insulator-semiconductor (MIS) stack. The 2D semiconductor layer at the top of the stack is the working electrode in a typical three-electrode electrochemical setup, as shown in Figure 1a, and the metal at the back of stack, called the "gate," serves as an independently controlled fourth electrode. Because the semiconductor and gate are capacitively coupled in the MIS stack, a voltage $V_{\rm G}$ applied between them results in electron accumulation or depletion in the semiconductor, depending on the sign and magnitude of V_G . Importantly, the gate-induced electron density in the semiconductor occurs independently of, and in summation with, the electron accumulation or depletion caused by the electrochemical potential $V_{\rm W}$ applied between the semiconductor and the reference electrode in the electrolyte (Figure 1a). In other words, V_G and V_W work in tandem to control the charge density in the thin semiconductor layer. The "backside" $V_{\rm G}$ charges up the MIS stack, while the "frontside" $V_{\rm W}$ charges up the electrochemical double layer, and the MIS stack and the double layer function as two capacitors coupled in series.

Our previous reports described this four-terminal electrochemistry using 2D MoS₂, graphene, and ultrathin ZnO (<5 nm) working electrodes, and we demonstrated enhancement of both outer-sphere^{1–5} and inner-sphere⁶ Faradaic reaction rates. To achieve more gating power, i.e., larger electron accumulations at simultaneously lower $V_{\rm G}$ values, ^{7,8} we implemented high dielectric constant HfO₂ as the insulator in the MIS stack. This allowed us to achieve up to a 30-fold increase in the electron transfer rate to outer-sphere redox couples from a 5 nm ZnO back-gated electrode at $V_{\rm G}$ values less than 8 V, for example.³ Collectively, these early demonstrations, and those of others, ^{9–18} have encouraged us to continue exploring the utility of back-gated 2D working electrodes for enhancing electrochemical reaction rates.

Here, we expand on these prior studies to further demonstrate that the four-electrode electrochemical system serves as a platform to investigate the fundamentals of non-Faradaic electrochemical processes on semiconductors. We

Received: October 30, 2023 Revised: December 10, 2023 Accepted: January 4, 2024 Published: January 18, 2024





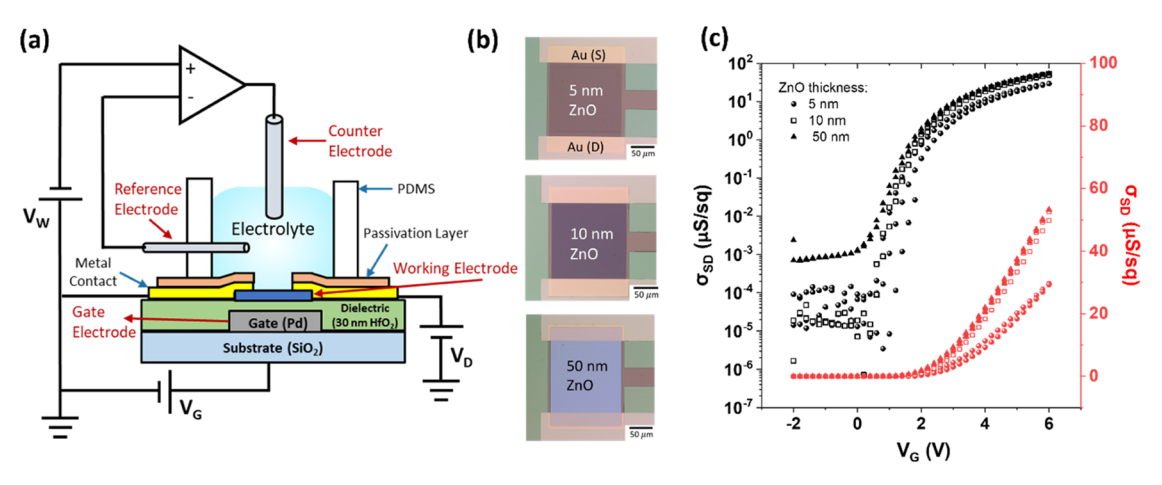


Figure 1. (a) Schematic of the four-terminal electrochemical cell with (b) optical images of the semiconductor ZnO working electrode with thicknesses of 5, 10, and 50 nm. (c) Sheet conductance of the semiconductor electrodes versus thickness and applied gate voltage (V_G) , with a V_G sweep rate of 0.2 V/s and an applied V_D of 0.1 V.

focus on thin back-gated ZnO electrodes, with which we have extensive experience, as shown in Figure 1. ZnO is a wellknown n-type semiconductor that can be deposited with precisely controlled thicknesses in the nanometer regime using atomic layer deposition (ALD). We have four principal results. First, by examining the lateral sheet conductance of the back-gated ZnO electrode in contact with the electrolyte (as shown in Figure 1a) as a function of both its thickness and the applied voltages $V_{\rm G}$ and $V_{\rm W}$, we are able to estimate the ZnO thickness range where the MIS and double-layer capacitors are intimately coupled. This is important because beyond this critical thickness, the back-gate voltage V_G will not impact electrochemistry on the top surface of the semiconductor, as will be explained. Second, by measuring the equilibrium electrochemical potential of the ZnO film (V_{ZnO}) as a function of V_G , we show that V_G directly modulates the electrochemical potential of the 2D semiconductor; that is, V_G provides independent electrochemical potential control of the ZnO film, which greatly clarifies its utility. Third, we demonstrate that from measurements of $V_{\rm ZnO}$ vs $V_{\rm G}$ we can extract the quantum capacitance CQ of the ultrathin ZnO film. CQ reflects the electronic density of states (DOS) of the semiconductor, and thus, this measurement serves as a kind of electronic spectroscopy. Fourth, we show that we can combine the measurements above to disentangle the two principal components of electrochemical potential, namely, the Fermilevel shift $\Delta\delta$ in the ZnO DOS and the double-layer charging energy $e\Delta\phi_{\rm EDL}$.^{22–24} We believe that this latter point will be critical in future studies of electrocatalysis where it is typically not known whether large overpotentials are mainly due to the need for a particular electron filling in the DOS (i.e., a particular $\Delta\delta$) or a certain interfacial electric field proportional to $\Delta\phi_{\rm EDL}$. Overall, we demonstrate that back-gated working electrodes establish new opportunities to understand fundamental electronic and non-Faradaic electrochemical processes at semiconductor-electrolyte interfaces.

MATERIALS AND METHODS

Materials. A p-doped Si wafer with 300 nm thermally grown oxide purchased from Silicon Valley Microelectronics was used as the substrate for device fabrication. Tetrakis-(dimethylamido)hafnium (TDMAH) and diethylzinc (DEZ) purchased from Sigma-Aldrich were used as the ALD

precursors for growing HfO₂ (as-grown dielectric constant $k \approx 16$) and ZnO ($k \approx 8$), respectively. Sylgard 184 silicone elastomer kit (including the base and curing agent) purchased from Fisher Scientific was used to fabricate the polydimethylsiloxane (PDMS) reservoir blocks. An SU8 2005 photoresist with an SU8 developer (Kayaku Advanced Materials) was employed for gold electrode passivation. Tetrabutylammonium hexafluorophosphate (TBAP, $\geq 99\%$) and acetonitrile (MeCN, anhydrous, 99.8%) purchased from Sigma-Aldrich were used as the electrolyte solution. A platinum wire (99.99%) with a 500 μ m diameter (Sigma-Aldrich) was used as the counter electrode. The Ag/Ag⁺ reference electrode (BASi Co.) was filled with 10 mM AgNO₃ (Sigma-Aldrich) and 0.1 M TBAP in MeCN. All chemicals were used without further purification.

Device Fabrication. The fabrication of the high-k localgate ZnO field-effect transistor (FET) device followed procedures described in detail in prior work.3 Briefly, a SiO₂/p-Si substrate was first prepatterned using photolithography to achieve a local-gate structure. Next, a 20 nm thick Pd layer (on 3 nm of Cr) was deposited on the substrate using electron beam evaporation (Evaporator CHA, SEC 600), followed by lift-off to achieve the local-gate electrode. The local-gate structure helps to reduce leakage current and increase the breakdown strength of the devices. Next, a 30 nm layer of hafnium oxide (HfO₂) was grown as the dielectric by using plasma-enhanced atomic layer deposition (PEALD) (Fiji G2). The PEALD process involved 230 cycles of alternating 250 ms pulses of TDMAH and oxygen plasma (300 W) for 6 s, with nitrogen purge between the pulses. The growth temperature was 150 °C.

To avoid contamination of the interface, a layer of ZnO was immediately deposited after HfO_2 deposition. The ZnO layer was grown using atomic layer deposition (ALD) at 200 °C for 50, 90, and 400 cycles, respectively, to achieve 5, 10, and 50 nm ZnO films (see Figure S1 in the Supporting Information). DEZ and H_2O were the precursors. Note that the 50 nm ZnO film was annealed at 400 °C in O_2 for 15 min in a rapid thermal annealer (RTA-600s) after deposition to achieve the desired I-V characteristics of the device. Annealing studies on 50 nm ZnO FETs are shown in Figure S2 in the Supporting Information. The deposited ZnO film was wet-etched in dilute acid solution HCI/H_2O of 1:1000 v/v). After that, the HfO_2

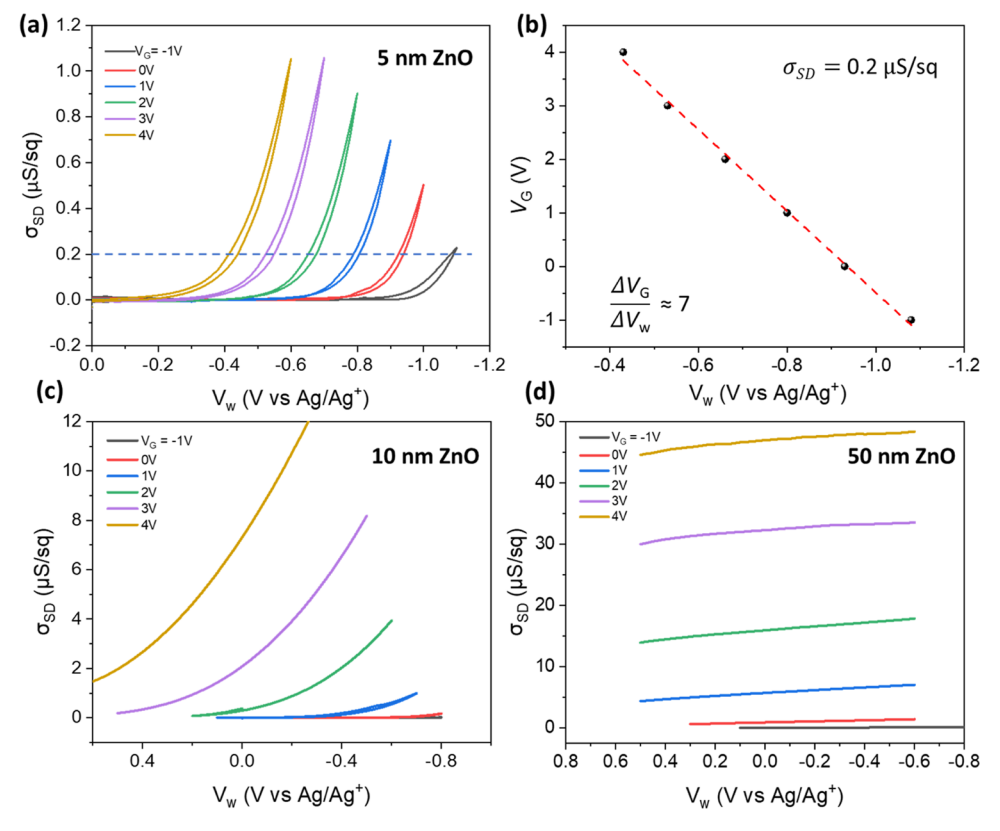


Figure 2. (a) Sheet conductance $\sigma_{\rm SD}$ of the 5 nm ZnO film as a function of $V_{\rm W}$ and $V_{\rm G}$. Film is in contact with the 0.1 M TBAP/MeCN electrolyte; $V_{\rm W}$ sweep rate is 20 mV/s and $V_{\rm D}=10$ mV. (b) Plot of $V_{\rm G}$ vs $V_{\rm W}$ at a fixed $\sigma_{\rm SD}=0.2~\mu{\rm S/sq}$ for the 5 nm ZnO electrode (see horizontal blue dashed line in panel (a)). The linear dependence reflects strong coupling of front and back sides of the ZnO electrode. (c) and (d) $\sigma_{\rm SD}$ of the 10 and 50 nm ZnO films, respectively, as a function of $V_{\rm W}$ and $V_{\rm G}$.

layer was plasma etched (Oxford Etcher, 180-ICP), with BCl₃/Ar gas flowing at a rate of 20:5 sccm, an RF power of 100 W, and a pressure of 2 mTorr, for a duration of 15 s. Finally, a lithographically patterned electrode layer of Ti/Au with thicknesses of 5/30 nm was deposited on the sample using electron beam evaporation, followed by a lift-off in acetone overnight. Devices with ZnO thicknesses of 5, 10, and 50 nm were fabricated in this manner.

After fabrication, the frontside of the device was passivated by an epoxy-based photoresist, SU8 2005. The devices were patterned by photolithography with only the ZnO and contact electrodes exposed. Finally, a PDMS block was fabricated by curing the Sylgard 184 silicone elastomer, followed by punching a reservoir with $d=4\,$ mm in the block. The PDMS reservoir was contact-bonded to the device after O_2 plasma activation of the PDMS surface.

Electrochemical Measurements. The four-terminal electrochemical measurement with simultaneous back-gating and electrolyte-gating was performed using the configuration shown in Figure 1a. Measurements were taken in ambient conditions using a probe station and a series of Keithley source measure units. A Pt wire ($d=0.5~\mathrm{mm}$) counter electrode and an Ag/Ag⁺ reference electrode were used. The ZnO channel in contact with the electrolyte functioned as the working electrode. A voltage ($V_{\rm W}$) was applied between working and reference electrodes where the current flowed through the working and counter electrodes. Meanwhile, $V_{\rm D}$ was applied between source and drain electrodes, while $V_{\rm G}$ was applied between the gate and source electrodes. The sheet

conductance was calculated by using the measured source to drain current $I_{\rm D}$.

The configuration for electrochemical potential measurements is illustrated in Figure 4a. Here, the counter electrode was not used. The working electrode was grounded, and the reference electrode was connected to a high-impedance voltmeter which measured the reference potential with respect to the grounded working electrode upon sweeping $V_{\rm G}$. In this setup, $I_{\rm G}$ and $\sigma_{\rm SD}$ can be simultaneously measured. Before the electrochemical measurements, the electrolyte solution was purged with N₂ for 15 min.

RESULTS AND DISCUSSION

Back-Gating of ZnO Working Electrodes with Different Thicknesses in the Absence and Presence of a Frontside Electrolyte. Optical images of gated ZnO electrodes with film thicknesses of 5, 10, and 50 nm are shown in Figure 1b. Because there are Ti/Au source and drain contacts to each ZnO electrode (Figure 1a,b) the Pd/HfO₂/ ZnO stack can function as a field-effect transistor (FET), where the in-plane sheet conductance σ_{SD} of the ZnO film is measured as a function of $V_{\rm G}$. ^{25,26} In Figure 1c, $\sigma_{\rm SD}$ is plotted vs $V_{\rm G}$ for all three ZnO thicknesses. All films are n-type; i.e., mobile electrons accumulate in ZnO with positive V_G values. Furthermore, σ_{SD} is very sensitive to V_{G} , increasing by up to 10^6 fold between $V_G = 0$ and +6 V. The higher sheet conductances in the 10 and 50 nm films reflect higher fieldeffect electron mobilities ($\mu = 25 \text{ cm}^2\text{V}^{-1}\text{s}^{-1}$) in these films than in the 5 nm ZnO films ($\mu = 15 \text{ cm}^2\text{V}^{-1}\text{s}^{-1}$), which is perhaps attributable to film morphology differences.

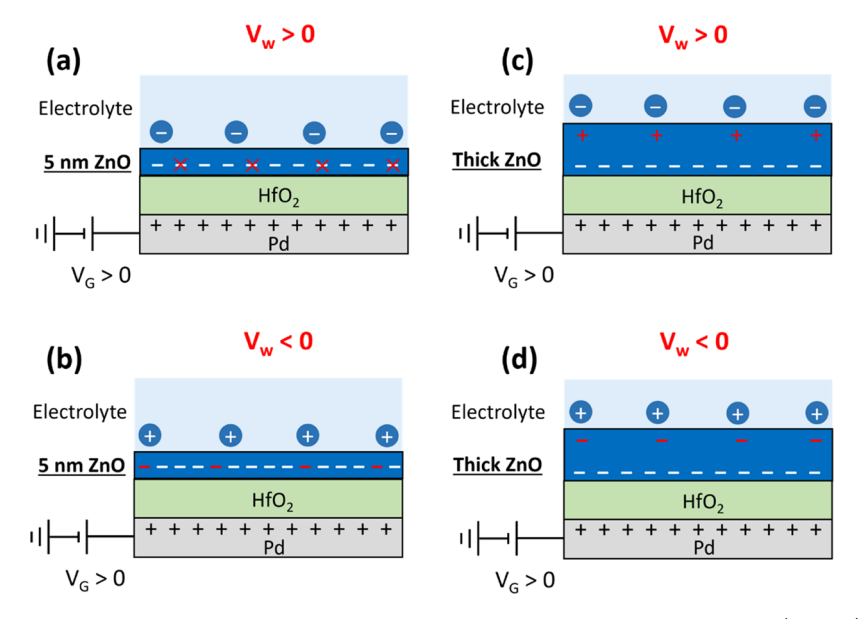


Figure 3. Scheme of charge accumulations at the ZnO-electrolyte interface under simultaneous back-gating ($V_G > 0$) and electrolyte-gating for thin 5 nm (a, b) and thicker (c, d) ZnO electrodes. Note that $V_W > 0$ for panels (a) and (c) and $V_W < 0$ for panels (b) and (d). $V_G > 0$ for all panels.

The back-gated sheet conductances of the 5, 10, and 50 nm ZnO electrodes were also measured while they were in contact with the electrolyte (0.1 M TBAP in MeCN), but with no applied electrochemical potential $V_{\rm W}$ (see Figure S3 in the Supporting Information). The σ_{SD} vs V_{G} behavior of ZnO in the presence of the electrolyte was similar to that shown in Figure 1c in the absence of the contacting electrolyte. However, a slight increase of hysteresis was observed for the 5 nm ZnO film in contact with the electrolyte. This is attributed to the influence of ions in the electrolyte and the formation of a weak double layer at the ZnO-electrolyte interface because of incomplete screening of the back-gate field by the electronic charge in the ZnO layer. Electrostatically bound anions can then interfere with electron transport in ZnO when the layer is ultrathin, leading to lower currents on the backward $V_{\rm G}$ sweep. We return to this point later.

Next, we examine the in-plane $\sigma_{\rm SD}$ behavior of the ZnO electrodes, in contact with the electrolyte, as a function of V_G and $V_{\rm W}$ applied simultaneously. Figure 2a displays $\sigma_{\rm SD}$ vs $V_{\rm W}$ for the 5 nm ZnO electrode back-gated with six different values of $V_{\rm G}$ ranging from $V_{\rm G} = -1$ V to +4 V. At a given $V_{\rm G}$ value, $\sigma_{\rm SD}$ of ZnO increased as $V_{\rm W}$ was swept to negative values, indicating electrons accumulated in the ZnO film at negative electrochemical potentials, as expected. Importantly, for increasingly positive $V_{
m G}$ values, the $\sigma_{
m SD}$ vs $V_{
m W}$ curves systematically shifted to the left, i.e., to more positive $V_{
m W}$ values. This means that at large V_G values, smaller (less negative) $V_{\rm W}$ bias is required to achieve the same $\sigma_{\rm SD}$. Note that positive $V_{\rm G}$ results in electron accumulation: it is simply a difference in sign convention that $V_{\rm G}$ > 0 and $V_{\rm W}$ < 0 both correspond to electron accumulation in ZnO. Figure 2b shows the $V_{\rm G}$ vs $V_{\rm W}$ relationship explicitly; $V_{\rm G}$ is plotted vs $V_{\rm W}$ for a fixed value of the lateral sheet conductance in ZnO, i.e., σ_{ZnO} = 0.2 μ S. The relationship is precisely linear and demonstrates that large $V_{\rm G}$ values mean only a small $V_{\rm W}$ is required, and vice versa, to achieve the same conductance. Selection of other $\sigma_{
m SD}$ values would lead to a set of parallel lines in this plot.

The linear behavior in Figure 2b indicates that the front (double-layer) and back (MIS) capacitors are closely coupled.

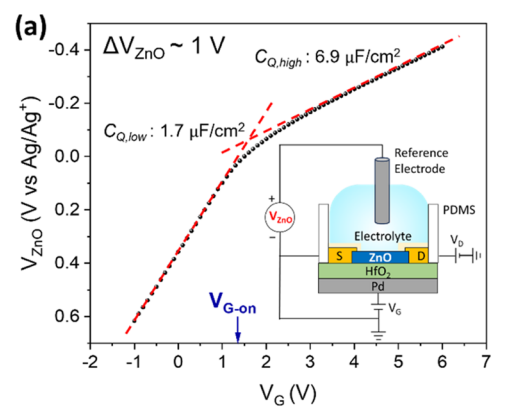
This coupling can be expressed mathematically by considering a charge balance on the ZnO film. At a fixed sheet conductance $\sigma_{\rm ZnO}$, the corresponding electronic charge Q on the ZnO film is the sum of charge induced across the MIS stack on the backside and the charge associated with the electrochemical double layer on the frontside. Thus,

$$Q = -V_{\rm W}C_{\rm EDL} + V_{\rm G}C_{\rm G} \tag{1}$$

where $C_{\rm EDL}$ and $C_{\rm G}$ are the double-layer capacitance and HfO₂ gate dielectric capacitance, respectively. Under the assumption that fixed $\sigma_{\rm SD}$ is equivalent to fixed Q, eq 1 predicts that the slope of the $V_{\rm G}$ vs $V_{\rm W}$ plot is $C_{\rm EDL}/C_{\rm G}$. We find from Figure 2b that the slope is 7, and estimating $C_{\rm G}=0.6~\mu{\rm F/cm^2}$, we obtain $C_{\rm EDL}=4.2~\mu{\rm F/cm^2}$, which is reasonable for an electric double layer. ^{27,28} Thus, the sheet conductance analysis for the 5 nm ZnO film is internally consistent and demonstrates that for this ultrathin ZnO layer, the $V_{\rm G}$ and $V_{\rm W}$ potentials are well coupled. According to eq 1, the linear behavior in Figure 2b also indicates that $C_{\rm EDL}$ and $C_{\rm G}$ are both independent of voltage.

The situation changes significantly as the ZnO electrode thickness increases. Figure 2d shows $\sigma_{\rm ZnO}$ vs $V_{\rm W}$ for the thickest 50 nm ZnO films at different $V_{\rm G}$ values. One can see that the measured $\sigma_{\rm ZnO}$ is strongly dependent on $V_{\rm G}$ but almost completely independent of $V_{\rm W}$; i.e., the slopes of the traces are close to zero. Stated another way, it is clear from Figure 2d that at any given $V_{\rm G}$ value, $V_{\rm W}$ is not able to shut off the sheet conductance of ZnO, whereas positive $V_{\rm W}$ values clearly caused $\sigma_{\rm ZnO}$ to collapse to near zero for the 5 nm electrode (Figure 2a). Thus, for the 50 nm electrode, $V_{\rm W}$ and $V_{\rm G}$ are not strongly coupled. Figure 2c displays the intermediate case, namely, the 10 nm ZnO electrode. There, increasing $V_{\rm G}$ shifts the $\sigma_{\rm ZnO}$ vs $V_{\rm W}$ curves more positive, but the overall $V_{\rm W}$ dependence is weaker than that shown in Figure 2a, and full shut off of $\sigma_{\rm ZnO}$ at positive $V_{\rm W}$ is hard to achieve at the most positive $V_{\rm G}$ values.

Schemes of the charge accumulation in thin and thick ZnO electrodes are depicted in Figure 3. Figure 3a shows the case where $V_{\rm G} > 0$ and $V_{\rm W} > 0$. In this case, the backside gate induces electrons in the 5 nm ZnO, but the electrochemical (double-layer) gate depletes electrons. The two competing



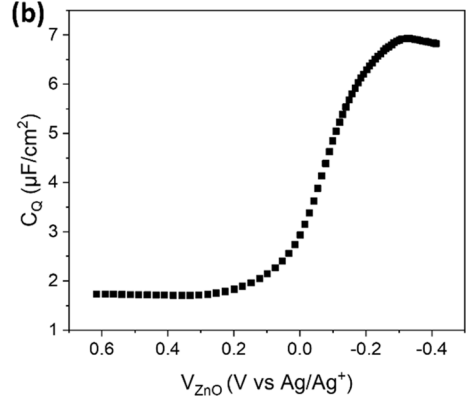


Figure 4. (a) Electrochemical potential $V_{\rm ZnO}$ of the 5 nm ZnO electrode with respect to the Ag/Ag⁺ reference electrode measured while backgating using the setup shown in the inset. The $V_{\rm G}$ sweep rate is 1 V/s. The red dashed lines are fits to the data using eq 2 and show the change of slope before and after the device was turned on. (b) Quantum capacitance $C_{\rm Q}$ vs $V_{\rm ZnO}$ obtained from the data in panel (a) using eq 2.

processes lead to reduced electron density in the 5 nm ZnO compared to the application of $V_{\rm G}$ alone. Figure 3b depicts the case where $V_{\rm G} > 0$ and $V_{\rm W} < 0$. Now, the front and back gates work together to boost the net electron density in the 5 nm ZnO film beyond what can be accumulated by $V_{\rm G}$ alone. These scenarios rationalize the data shown in Figure 2a for ultrathin 5 nm ZnO films.

On the other hand, Figure 3c,d shows the expected situations for the 50 nm thick ZnO films. One can see in Figure 3c,d that the charges induced by the electrical double layer (shown in red) are spatially separated from the charges induced by the back-gate (shown in white). The front and back capacitors are decoupled, and this means that $V_{\rm W}$ has little influence on the accumulated electron density induced by $V_{\rm G}$. Stated in another way, there is no depletion of mobile electrons for any positive value of $V_{\rm W}$ and one predicts that the sheet conductance is weakly affected by $V_{\rm W}$, which is what we observe in Figure 2d.

Determining the ZnO Equilibrium Potential (V_{ZnO}) vs V_G and Quantum Capacitance (C_Q). Next, instead of applying the working electrode potential V_W , we measured the electrochemical potential on ZnO electrodes (denoted as $V_{\rm ZnO}$) with respect to the reference electrode (Ag/Ag⁺) while sweeping V_G . Figure 4a shows V_{ZnO} vs V_G data for a 5 nm thick ZnO electrode, and the electrical setup for this measurement is depicted in the inset. The first observation in Figure 4a is that for a $V_{\rm G}$ range of -1 to +6 V, or 7 V total, $V_{\rm ZnO}$ varies by nearly 1 V from +0.55 to -0.4 V vs Ag/Ag⁺. This is a critical result: it says that $V_{\rm G}$ provides direct control of the electrochemical potential of the thin ZnO film and that large changes in electrochemical potential, of order 1 V, are accessible by means of back-gating. The second observation is that two domains are evident in Figure 4a plot. At low $V_{\rm G}$ values, $V_{\rm ZnO}$ increases strongly (becomes more negative) with increasing $V_{\rm G}$. However, near $V_{\rm G}$ = +1.5 V, there is a slope change. For $V_{\rm G}$ > + 1.5 V, $V_{\rm ZnO}$ continues to become more negative but does so more slowly.

It can be shown (see the Supporting Information) that the slope of the $V_{\rm ZnO}$ vs $V_{\rm G}$ plot is directly related to the capacitance of the HfO₂ dielectric $C_{\rm G}$ and the quantum capacitance $C_{\rm Q}$ of the ZnO film:

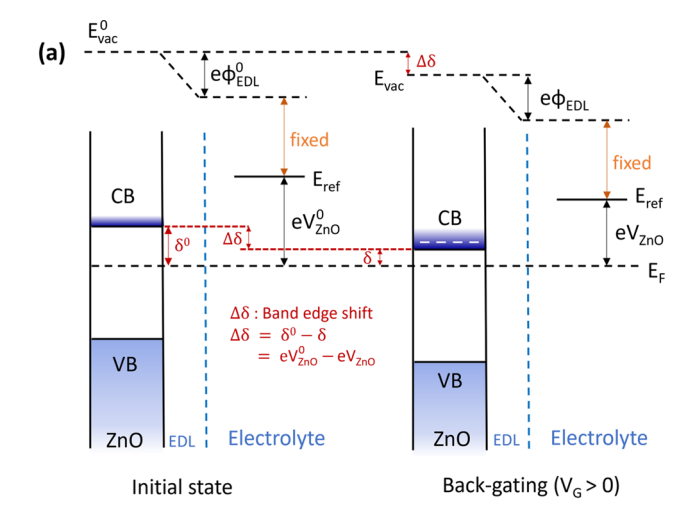
$$\frac{\mathrm{d}V_{\mathrm{ZnO}}}{\mathrm{d}V_{\mathrm{G}}} = -\frac{1}{1 + \frac{c_{\mathrm{Q}}}{c_{\mathrm{G}}}} \tag{2}$$

where $C_{\rm Q}$ is the intrinsic capacitance of a material due to its electronic density of states ($C_{\rm Q}={\rm e}^2\cdot{\rm DOS}$). For typical metal/insulator/metal capacitors, $C_{\rm Q}^{\rm metal}\gg C_{\rm G}^{\rm insulator}$ and the derivative in eq 2 is effectively zero. However, for an ultrathin film semiconductor on a high-capacitance dielectric, $C_{\rm G}$ can be on the same order of magnitude as $C_{\rm Q}$. This is the situation here. $C_{\rm G}^{\rm HfO2}=0.6~\mu{\rm F/cm}^2$, which is a large value fixed by the dielectric constant and thickness of the HfO₂ layer. From straight line fits to the two domains in Figure 4a, we extract $C_{\rm Q,low}^{\rm ZnO}=1.7~\mu{\rm F/cm}^2$ and $C_{\rm Q,high}^{\rm ZnO}=6.9~\mu{\rm F/cm}^2$ using eq 2. The abrupt slope change evident in Figure 4a is caused by an abrupt change in $C_{\rm Q}^{\rm ZnO}$ at approximately $V_{\rm G}=+1.5~{\rm V}$ or $V_{\rm ZnO}\sim0~{\rm V}~{\rm vs}~{\rm Ag/Ag}^+$. Figure 4b displays the continuous variation in $C_{\rm Q}^{\rm ZnO}$ vs $V_{\rm ZnO}$ obtained from panel (a) using eq 2. It is clear that there is a step change in $C_{\rm Q}^{\rm ZnO}$ as $V_{\rm ZnO}$ is varied.

We can understand the changes in the $C_{\rm O}^{\rm ZnO}$ in this way. At low $V_{\rm G}$ values, the Fermi level $E_{\rm F}$ of the ZnO film is deep in the ZnO band gap where the density of electronic states (DOS) should be low (the only in-gap states are localized trap states). As $V_{\rm G}$ swings positive, the field effect causes the conduction band edge to shift down, or equivalently, in the language of electrochemists one can say the Fermi level moves up toward the conduction band edge. Because the DOS is low, C_{O}^{ZnO} is low, and small changes in $V_{\rm G}$ produce relatively large gains in $V_{\rm ZnO}$. However, once the conduction band to $E_{\rm F}$ offset (δ) becomes small enough, the channel opens, electrons accumulate in the conduction band, and the DOS near $E_{\rm F}$ is much higher. Consequently, the $C_{\rm Q}^{\rm ZnO}$ is higher. This means that beyond $V_G = +1.5 \text{ V}$, V_{ZnO} is less sensitive to V_G (i.e., more electrons can accumulate at a given energy because the DOS is high). We note that the σ_s vs V_G plot in Figure 1c also shows that the threshold voltage V_T for the onset of conduction is \sim + 1.5 V; Figure 1c is consistent with the data in Figure 4a,b.

Separating Band Edge Shift $\Delta\delta$ from Double-Layer Charging Energy $e\Delta\phi_{\text{EDL}}$. We have shown above that the back-gate controls the electrochemical potential of the ZnO film. In this last section, we consider the fundamental differences between back-gating and normal electrochemical gating in our four-electrode cell.

Figure 5a,b depicts the energy-level diagrams for back-gating and frontside electrochemical gating, respectively. Considering Figure 5a first, application of a back-gate voltage $V_{\rm G}$ pulls the conduction band edge down toward the system Fermi level $E_{\rm F}$ via the field effect. The initial offset between the conduction band and $E_{\rm F}$ is δ^0 (see the "initial state" in Figure 5a).



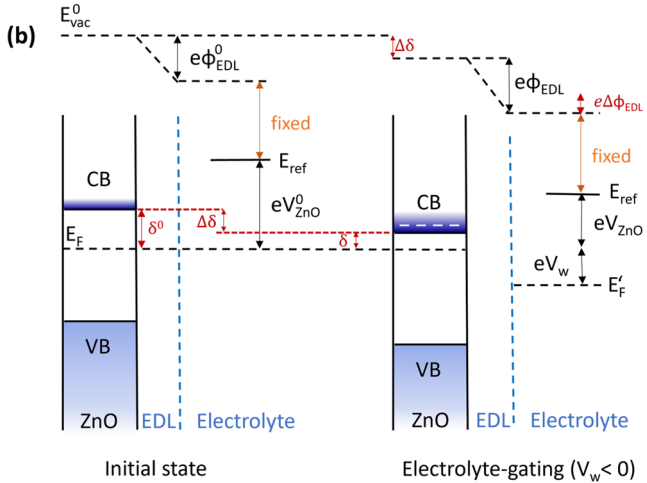


Figure 5. Energy-level diagram of the ultrathin ZnO electrode-electrolyte interface. (a) Initial and final states under back-gating where $V_{\rm G}>0$ V is applied across the Pd/HfO₂/ZnO capacitor. The voltage drop across the MIS capacitor is not shown; only the ZnO-electrolyte interface is shown. (b) Initial and final states for frontside electrochemical gating with $V_{\rm W}<0$. In both panels (a) and (b), δ^0 and δ are the conduction band offsets from the Fermi level $E_{\rm F}$ in the initial state and final states, respectively; $\Delta\delta$ is the band edge shift; $V_{\rm ZnO}^{\rm C}$ and $V_{\rm ZnO}$ are the equilibrium potentials of ZnO versus the reference $E_{\rm ref}$; $\phi_{\rm EDL}$ is the double-layer potential; and $E_{\rm vac}^0$ is the vacuum level. Blue shading in the conduction bands (CB) and valence bands (VB) indicates the electron energy distribution.

Application of $V_{\rm G} > 0$ shrinks the band edge offset from δ^0 to δ . $E_{\rm F}$ is fixed across the whole system because the ZnO film and the reference electrode are in equilibrium $(V_{\rm W}=0)$.

The band edge shift is given by the difference in band edge position before and after $V_{\rm G}$ is applied, i.e., $\Delta\delta=\delta^0-\delta$. Correspondingly, $V_{\rm ZnO}$ measures the position of $E_{\rm F}$ relative to the fixed Ag/Ag⁺ reference electrode. Initially, the electrochemical potential is $V_{\rm ZnO}^0$. Upon back-gating, the equilibrium potential shifts to $V_{\rm ZnO}$. From the diagram, one can work out that

$$\Delta \delta = \delta^0 - \delta = e(V_{Z_{DO}}^0 - V_{Z_{DO}}) \tag{3}$$

Equation 3 expresses the important idea that the equilibrium electrochemical potential $V_{\rm ZnO}$ can be used to measure the band edge shift $\Delta\delta$. The significance of $\Delta\delta$ is that it determines the electron density in the conduction band via the DOS and

the Fermi function; a large $\Delta\delta$ (small δ) means large electron accumulations.

Turning now to the electrochemical gating picture in Figure 5b, $V_{\rm G}=0$ but $V_{\rm W}<0$. Negative $V_{\rm W}$ brings cations to the ZnO–electrolyte interface, as electrons accumulate on the ZnO layer, charging up the double layer. Charging the double layer has two effects: (i) it results in an increase in the double-layer potential drop $\Delta\phi_{\rm EDL}=\phi_{\rm EDL}^{\circ}-\phi_{\rm EDL}$ between the initial and final states and (ii) it causes the conduction band edge to shift down by $\Delta\delta$. Using an energy balance, we can capture these two effects mathematically: $^{3Z-34}$

$$eV_{\rm W} = \Delta\delta + e\Delta\phi_{\rm EDL} \tag{4}$$

That is, the energy provided by the external circuit supplying eV_W is the sum of the band edge shift for ZnO and the double-layer charging energy. In Figure 5b, $E_{\rm F}$ is not constant across the semiconductor—electrolyte interface because of the applied electrochemical potential V_W .

For comparison, we can write a similar equation for backgate charging, i.e.,

$$eV_{\rm G} = \Delta \delta + e \Delta \phi_{\rm dielectric} \tag{5}$$

where $e\Delta\phi_{\rm dielectric}$, which is not depicted in Figure 5, is the energy invested in polarizing the insulator layer in the MIS stack. We see in eqs 4 and 5 the symmetry of the back-gate and conventional electrochemical control: in both cases, the supplied electrical energy produces band edge shifts and material polarization (double layer vs dielectric). A critical point, however, is that for back-gating we can isolate $\Delta\delta$ in eq 5 via measurements of $V_{\rm ZnO}$ and eq 3, so we can directly compare $\Delta\delta$ and $e\Delta\phi_{\rm dielectric}$ for a given $V_{\rm G}$. At first glance, it seems that we do not have the same opportunity to know the relative magnitudes of $\Delta\delta$ and $e\Delta\phi_{\rm EDL}$ in eq 4 because we do not have independent measures of either $\Delta\delta$ or $e\Delta\phi_{\rm EDL}$.

However, it turns out that we can indeed disentangle $\Delta\delta$ and $e\Delta\phi_{\rm EDL}$ by using two distinct experiments. In the first experiment, we measure the in-plane sheet conductance σ_{SD} of ZnO vs $V_{\rm W}$ (i.e., applied electrochemical potential), keeping $V_{\rm G}$ = 0 V. In the second experiment, we measure both $\sigma_{\rm SD}$ and the equilibrium electrochemical potential $V_{\rm ZnO}$ of the ZnO film while sweeping $V_{\rm G}$. Plots of $\sigma_{\rm SD}$ vs $V_{\rm W}$ and $\sigma_{\rm SD}$ vs $V_{\rm ZnO}$ are then overlaid. Because $V_{
m W}$ and $V_{
m ZnO}$ are on the same scale, i.e., one is the applied electrochemical potential and the other is the measured equilibrium potential versus the same reference, the x-axes are interchangeable. Figure 6 shows the example data. The two curves have been shifted to align the sheet conductances just at channel turn on. Figure 6 shows that a higher potential is required in the red trace (electrochemical gating only) to achieve the same $\sigma_{ ext{SD}}$ as in the black trace (back-gating only). The reason is that $\sigma_{
m SD}$ in the black trace hinges only on the band offset change $\Delta \delta$, which sets the electron distribution in ZnO. For the red trace, on the other hand, the potential at the same $\sigma_{\rm SD}$ value reflects the sum of $\Delta\delta$ /e and $\Delta\phi_{\rm EDL}$ (eq 4). Making the reasonable assumption that $\Delta \delta$ is the same for the two traces at the same $\sigma_{SD} = 0.1 \ \mu S$ (this is equivalent to saying that the electron densities in ZnO are the same), we can take the shift in energy along the x-axis to be an approximate measure of $\Delta\phi_{\rm EDL}$, as shown. Importantly, one sees that $\Delta\phi_{\mathrm{EDL}}$ is similar in magnitude to $\Delta\delta/\mathrm{e}$, i.e., $\Delta\phi_{\mathrm{EDL}} \approx \Delta\delta/\mathrm{e} \approx 0.1$ V. In other words, for electrochemical gating about half the electrochemical energy in the applied $V_{\rm W}$ is spent on charging the double layer.

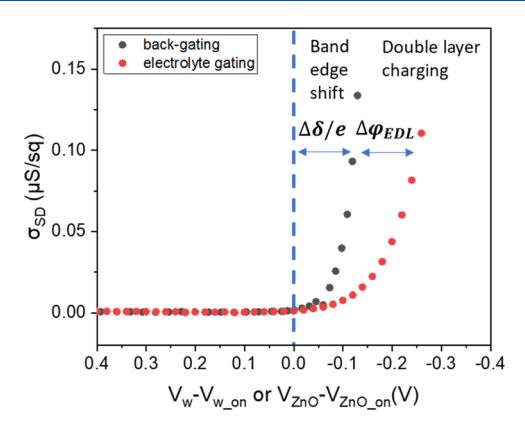


Figure 6. Sheet conductance of the 5 nm thick ZnO electrode vs electrochemical potential for two different experiments. In the first experiment (red trace), the sheet conductance was measured while the working electrode potential, $V_{\rm W}$, was swept. In the second experiment (black trace), sheet conductance and the electrochemical potential $V_{\rm ZnO}$ of the ZnO electrode were measured simultaneously, while the back-gate potential $V_{\rm G}$ was swept. The black trace is thus the measured sheet conductance versus the measured electrochemical potential, $V_{\rm ZnO}$, during back-gating. It is evident that a smaller change in the electrochemical potential of the ZnO electrode is required to achieve the same sheet conductance when back-gating versus normal potential $(V_{\rm W})$ control. This is because back-gating does not require full double-layer charging to achieve the same electron density, i.e., conductance. Note that the two traces are aligned at $V_{\rm w\ on}$ and $V_{
m ZnO~on}$, which are the potentials corresponding to the onset of electron conduction.

We note that the values extracted from Figure 6 are approximate and are subject to assumptions underlying eq 3. Equation 3 states that $e\Delta V_{\rm ZnO} = \Delta \delta$, but this is only true if back-gating does not result in any double-layer charging at the ZnO-electrolyte interface, i.e., $\phi_{\text{EDL}} \sim \phi_{\text{EDL}}$. If the ZnO screening length at a given electron concentration is larger than the thickness of ZnO, some back-gate field lines will penetrate through the ZnO layer into the electrolyte, where they will attract anions. In such a case, the measured $V_{\rm ZnO}$ will be larger than the actual $\Delta \delta/e$. Thus, $\Delta \delta/e$ will be overestimated by eq 3. Returning to our Figure 6 analysis, $\Delta\delta/e$ depicted is an upper limit, which means that $\Delta\phi_{\mathrm{EDL}}$ could be somewhat larger than indicated. More experiments are necessary to determine exactly what the ZnO thickness should be to have complete gate field screening in ZnO and no anion attraction (i.e., electric double-layer formation). Our sheet conductance measurements on the 5 nm ZnO electrode showed some hysteresis that we attributed to ion motion at the interface (Figure S3). Still, Figure 6 illustrates an important point, namely, that $\Delta\delta/e$ and $\Delta\phi_{\rm EDL}$ can be deconvoluted in principle. We speculate that in future experiments on electrocatalysis, one may be able to compare plots of reaction current versus $V_{\rm W}$ and $V_{\rm ZnO}$ simultaneously to assess the relative importance of $\Delta\delta/e$ vs $\Delta\phi_{
m EDL}$ to the required overpotential.

CONCLUSIONS

In conclusion, we have shown that the electrochemical potential ($E_{\rm F}$ position in the DOS) of a 5 nm thick ZnO semiconductor working electrode can be varied by nearly 1 V vs an Ag/Ag⁺ reference electrode by application of a 7 V gate bias between the ZnO and a capacitively coupled gate electrode. The gate bias $V_{\rm G}$ thus acts as an independent

control of the working electrode electrochemical potential that acts in tandem with conventional electrochemical potential $V_{\rm W}$. We have exploited this independent control in a four-terminal setup to make measurements of the quantum capacitance C_O of the ZnO film as a function of the Fermi-level position, a measurement that is difficult to achieve with a normal threeterminal experiment because of the convolution of doublelayer charging potential $\Delta\phi_{ ext{EDL}}$ with the Fermi-level shift potential $\Delta\delta/e$. We anticipate that $C_{\rm O}$ measurements, which represent a kind of spectroscopy, could be used to characterize the DOS of a variety of ultrathin semiconductor films, as has been reported for certain 2D materials. We have also used the four-terminal setup to explicitly deconvolute $\Delta\phi_{ ext{EDL}}$ and $\Delta\delta/e$ for different charge states of the ZnO electrode. Overall, ultrathin back-gated working electrodes appear promising for a fundamental understanding of the electronic and non-Faradaic electrochemical processes occurring at semiconductor-electrolyte interfaces.

ASSOCIATED CONTENT

Supporting Information

The Supporting Information is available free of charge at https://pubs.acs.org/doi/10.1021/acs.jpcc.3c07198.

ALD thin-film growth; electronic measurements on ZnO FETs; derivation of equations (PDF)

AUTHOR INFORMATION

Corresponding Author

C. Daniel Frisbie — Department of Chemistry, University of Minnesota, Minneapolis, Minnesota 55455, United States; Department of Chemical Engineering and Materials Science, University of Minnesota, Minneapolis, Minnesota 55455, United States; orcid.org/0000-0002-4735-2228; Email: frisbie@umn.edu

Author

Yuxin Wang – Department of Chemistry, University of Minnesota, Minneapolis, Minnesota 55455, United States; orcid.org/0000-0002-6590-6087

Complete contact information is available at: https://pubs.acs.org/10.1021/acs.jpcc.3c07198

Notes

The authors declare no competing financial interest.

ACKNOWLEDGMENTS

This work was primarily supported by the Department of Energy, Basic Energy Sciences Catalysis Program (DE-SC0021163). Parts of the work were carried out in the Characterization Facility at the University of Minnesota, which was partially supported by the NSF through the MRSEC program (DMR-2011401). Other portions of this work were conducted in the Minnesota Nano Center, which is supported by the National Science Foundation through the National Nano Coordinated Infrastructure Network (NNCI) under Award Number ECCS-2025124.

REFERENCES

(1) Kim, C. H.; Frisbie, C. D. Field Effect Modulation of Outer-Sphere Electrochemistry at Back-Gated, Ultrathin Zno Electrodes. *J. Am. Chem. Soc.* **2016**, *138* (23), 7220–7223.

- (2) Wang, Y.; Kim, C.-H.; Yoo, Y.; Johns, J. E.; Frisbie, C. D. Field Effect Modulation of Heterogeneous Charge Transfer Kinetics at Back-Gated Two-Dimensional MoS₂ Electrodes. *Nano Lett.* **2017**, *17* (12), 7586–7592.
- (3) Wang, Y.; Wang, Y.; Frisbie, C. D. Electrochemistry at Back-Gated, Ultrathin ZnO Electrodes: Field-Effect Modulation of Heterogeneous Electron Transfer Rate Constants by 30× with Enhanced Gate Capacitance. ACS Appl. Mater. Interfaces 2023, 15 (7), 9554–9562.
- (4) Kim, C. H.; Frisbie, C. D. Determination of Quantum Capacitance and Band Filling Potential in Graphene Transistors with Dual Electrochemical and Field-Effect Gates. *J. Phys. Chem. C* **2014**, *118* (36), 21160–21169.
- (5) Kim, C. H.; Wang, Y.; Frisbie, C. D. Continuous and Reversible Tuning of Electrochemical Reaction Kinetics on Back-Gated 2D Semiconductor Electrodes: Steady-State Analysis Using a Hydrodynamic Method. *Anal. Chem.* **2019**, *91* (2), 1627–1635.
- (6) Wang, Y.; Udyavara, S.; Neurock, M.; Frisbie, C. D. Field Effect Modulation of Electrocatalytic Hydrogen Evolution at Back-Gated Two-Dimensional MoS₂ Electrodes. *Nano Lett.* **2019**, *19* (9), 6118–6123.
- (7) Shim, J. H.; Choi, H. J.; Kim, Y.; Torgersen, J.; An, J.; Lee, M. H.; Prinz, F. B. Process-Property Relationship in High-K ALD SrTiO₃ and BaTiO₃: A Review. *J. Mater. Chem. C* **2017**, *5* (32), 8000–8013.
- (8) Ortiz, R. P.; Facchetti, A.; Marks, T. J. High-K Organic, Inorganic, and Hybrid Dielectrics for Low-Voltage Organic Field-Effect Transistors. *Chem. Rev.* **2010**, *110* (1), 205–239.
- (9) Yang, H.; He, Q.; Liu, Y.; Li, H.; Zhang, H.; Zhai, T. On-Chip Electrocatalytic Microdevice: An Eemerging Platform for Expanding the Insight into Electrochemical Processes. *Chem. Soc. Rev.* **2020**, 49 (10), 2916–2936.
- (10) He, Y.; He, Q.; Wang, L.; Zhu, C.; Golani, P.; Handoko, A. D.; Yu, X.; Gao, C.; Ding, M.; Wang, X.; et al. Self-Gating in Semiconductor Electrocatalysis. *Nat. Mater.* **2019**, *18* (10), 1098–1104.
- (11) Wang, J.; Yan, M.; Zhao, K.; Liao, X.; Wang, P.; Pan, X.; Yang, W.; Mai, L. Field Effect Enhanced Hydrogen Evolution Reaction of MoS₂ Nanosheets. *Adv. Mater.* **2017**, *29* (7), No. 1604464.
- (12) Wu, Y.; Ringe, S.; Wu, C. L.; Chen, W.; Yang, A.; Chen, H.; Tang, M.; Zhou, G.; Hwang, H. Y.; Chan, K.; Cui, Y. A Two-Dimensional MoS₂ Catalysis Transistor by Solid-State Ion Gating Manipulation and Adjustment (Sigma). *Nano Lett.* **2019**, *19* (10), 7293–7300.
- (13) Pan, Y.; Wang, X.; Zhang, W.; Tang, L.; Mu, Z.; Liu, C.; Tian, B.; Fei, M.; Sun, Y.; Su, H.; et al. Boosting the Performance of Single-Atom Catalysts Via External Electric Field Polarization. *Nat. Commun.* **2022**, *13* (1), No. 3063.
- (14) Ding, M.; He, Q.; Wang, G.; Cheng, H. C.; Huang, Y.; Duan, X. An on-Chip Electrical Transport Spectroscopy Approach for in Situ Monitoring Electrochemical Interfaces. *Nat. Commun.* **2015**, *6* (1), No. 7867
- (15) Chen, J.; Lu, N.; Zhao, Y.; Huang, J.; Gan, X.; Chen, X.; Yang, Z.; Wen, Q.; Zhai, T.; Liu, Y. On-Chip Microdevice Unveils Reactant Enrichment Effect Dominated Electrocatalysis Activity in Molecular-Linked Catalysts. *Nano Lett.* **2022**, 22 (24), 10154–10162.
- (16) Qi, J.; Wang, W.; Li, Y.; Sun, Y.; Wu, Z.; Bao, K.; Wang, L.; Ye, R.; Ding, M.; He, Q. On-Chip Investigation of Electrocatalytic Oxygen Reduction Reaction of 2d Materials. *Small* **2022**, *18* (47), No. 2204010.
- (17) Zhao, Y.; Huang, J.; Chen, J.; Gan, X.; Wen, Q.; Li, H.; Duan, J.; Chen, B.; Zhai, T.; Liu, Y. External-Field-Driven Molecular Polarization Manipulates Reactant Interface toward Efficient Hydrogen Evolution. *Sci. China Mater.* **2023**, *66* (9), 3501–3508.
- (18) Wang, J.; Qiu, M.; Jiang, Y.; Xia, H.; An, X.; Wang, S.; He, Y. Emerging on-Chip Microcells in Electrocatalysis: Functions of Window and Circuit. *EES Catal.* **2023**, *1*, 874–891.
- (19) Carcia, P. F.; McLean, R. S.; Reilly, M. H. High-Performance Zno Thin-Film Transistors on Gate Dielectrics Grown by Atomic Layer Deposition. *Appl. Phys. Lett.* **2006**, 88 (12), No. 123509.

- (20) Lim, S. J.; Kwon, S.; Kim, H. ZnO Thin Films Prepared by Atomic Layer Deposition and RF Sputtering as an Active Layer for Thin Film Transistor. *Thin Solid Films* **2008**, *516* (7), 1523–1528.
- (21) Tynell, T.; Karppinen, M. Atomic Layer Deposition of ZnO: A Review. Semicond. Sci. Technol. 2014, 29 (4), No. 043001.
- (22) Nozik, A. J.; Memming, R. Physical Chemistry of Semiconductor-Liquid Interfaces. *J. Phys. Chem. A* **1996**, *100* (31), 13061–13078.
- (23) Bard, A. J. F.; Faulkner, L. R.; White, Henry. *Electrochemical Methods: Fundamentals and Applications*, 2nd ed.; Wiley: New York, 2006
- (24) Morrison, S. R. Electrochemistry at Semiconductor and Oxidized Metal Electrodes.; Plenum Press: New York, NY: United States, 1980.
- (25) Zaumseil, J.; Sirringhaus, H. Electron and Ambipolar Transport in Organic Field-Effect Transistors. *Chem. Rev.* **2007**, *107* (4), 1296–1323
- (26) Choi, H. H.; Cho, K.; Frisbie, C. D.; Sirringhaus, H.; Podzorov, V. Critical Assessment of Charge Mobility Extraction in Fets. *Nat. Mater.* **2018**, *17* (1), 2–7.
- (27) Wu, J. Understanding the Electric Double-Layer Structure, Capacitance, and Charging Dynamics. *Chem. Rev.* **2022**, *122* (12), 10821–10859.
- (28) Li, D. D.; Li, E. C.; Yang, Y. R.; Wang, X. D.; Feng, G. Structure and Capacitance of Electrical Double Layers in Tricationic Ionic Liquids with Organic Solvents. *J. Phys. Chem. B* **2021**, 125 (46), 12753–12762.
- (29) Dröscher, S.; Roulleau, P.; Molitor, F.; Studerus, P.; Stampfer, C.; Ensslin, K.; Ihn, T. Quantum Capacitance and Density of States of Graphene. *Appl. Phys. Lett.* **2010**, *96* (15), No. 152104.
- (30) Berthod, C.; Zhang, H.; Morpurgo, A. F.; Giamarchi, T. Theory of Cross Quantum Capacitance. *Phys. Rev. Res.* **2021**, 3 (4), No. 043036.
- (31) Liang, Y.; Chang, H. C.; Ruden, P. P.; Frisbie, C. D. Examination of Au, Cu, and Al Contacts in Organic Field-Effect Transistors Via Displacement Current Measurements. *J. Appl. Phys.* **2011**, *110* (6), No. 064514.
- (32) Abbas, G.; Sonia, F. J.; Jindra, M.; Červenka, J.; Kalbáč, M.; Frank, O.; Velický, M. Electrostatic Gating of Monolayer Graphene by Concentrated Aqueous Electrolytes. *J. Phys. Chem. Lett.* **2023**, *14* (18), 4281–4288.
- (33) Das, A.; Pisana, S.; Chakraborty, B.; Piscanec, S.; Saha, S. K.; Waghmare, U. V.; Novoselov, K. S.; Krishnamurthy, H. R.; Geim, A. K.; Ferrari, A. C.; Sood, A. K. Monitoring Dopants by Raman Scattering in an Electrochemically Top-Gated Graphene Transistor. *Nat. Nanotechnol.* **2008**, 3 (4), 210–215.
- (34) Froehlicher, G.; Lorchat, E.; Berciaud, S. Charge Versus Energy Transfer in Atomically Thin Graphene-Transition Metal Dichalcogenide Van Der Waals Heterostructures. *Phys. Rev. X* **2018**, 8 (1), No. 011007.